

Article

# A Soft-Switching SEPIC with Multi-Output Sources

Cheng-Tao Tsai <sup>1,\*</sup> and Jye-Chau Su <sup>2</sup>

<sup>1</sup> Department of Electrical Engineering, National Chin-Yi University of Technology, Taichung 41170, Taiwan

<sup>2</sup> Department of Electronic Engineering, National Chin-Yi University of Technology, Taichung 41170, Taiwan; jc07@ms34.hinet.net

\* Correspondence: cttsai@ncut.edu.tw; Tel.: +886-4-23924505

Academic Editor: Mostafa Bassiouni

Received: 2 March 2017; Accepted: 3 May 2017; Published: 6 May 2017

**Abstract:** In this paper, a soft-switching single-ended-primary-inductance converter (SEPIC) with multi-output sources is proposed. The proposed SEPIC has the following advantages: (1) The conversion efficiency can be increased. To incorporate a soft-switching cell with a flyback-type, the power switches can achieve zero-voltage-switching (ZVS) and zero-current-switching (ZCS) features under turn-on transitions, resulting in reducing the switching losses and electromagnetic interference (EMI); (2) The applicability can be maximized. To apply the voltage ratio of the transformers, the proposed SEPIC has multi-output sources with step-up/down voltage functions. Finally, a prototype of the soft-switching SEPIC with multi-output sources is built and implemented. Simulated and experimental results are presented to verify the performance and the feasibility of the proposed soft-switching SEPIC with multi-output sources.

**Keywords:** soft-switching; SEPIC; ZVS; ZCS; EMI

---

## 1. Introduction

Industrial development and technological progress has resulted in fossil fuel energy shortages and serious air quality concerns. To overcome fossil fuel energy shortages, the demand for renewable energy sources has increased significantly. The typical renewable energy sources include Photovoltaic PV panels, wind energy, and fuel cells, which have the features of cleanliness and freedom [1]. However, renewable energy sources have instability and intermittent output power characteristics. Thus, they demand a switching-mode power converter to convert and regulate the energies into suitable utilization power to loads [2,3].

With the demands of lighter weight, higher efficiency, and smaller size, switching-mode power converters have been becoming essential parts of renewable energy systems. The voltage and current requirements of the renewable energy systems often differ radically from the forms in which the renewable energies are delivered or stored. Switching-mode power converters use power semiconductor devices to control the power flow in an efficient way. A number of non-isolated power converters have been developed and proposed; for example, Buck, Boost, 'Cuk, Zeta, and single-ended-primary-inductance converters (SEPIC), which have simple constructions and are widely used in low and medium power applications [4–6]. To step-up/down voltage and non-isolated applications, the SEPIC is widely used, as shown in Figure 1. However, the SEPIC has only a set of output sources, resulting in low applicability [7–9]. Furthermore, the high-frequency hard-switching conditions of the power switch (Metal-oxide-semiconductor-field-effect transistor, MOSFET) are major contributors to switching losses and high-frequency ringing in the SEPIC, resulting in high power losses, serious electromagnetic interference (EMI), and low conversion efficiency [8–10]. Figure 2 shows the experimental results of SEPIC with hard-switching conditions. High-frequency hard-switching of the high  $di/dt$  and  $dv/dt$  results in EMI of the high-frequency voltage and current, as well as high

switching losses across the power switch. The serious EMI and switching losses are considerable, which will damage the tolerance of the power switch [9–11]. Figure 3 shows the typical switching loci for a power switch without and with soft-switching techniques, respectively. To resolve these discussed problems, the SEPIC with soft-switching techniques and multi-output sources is a highly researched topic.

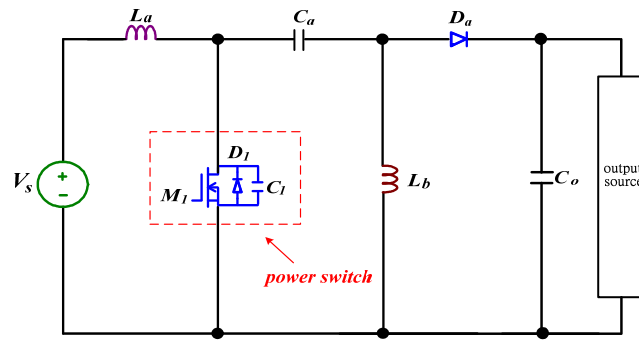


**Figure 1.** Topology of conventional SEPIC (single-ended-primary-inductance converter).

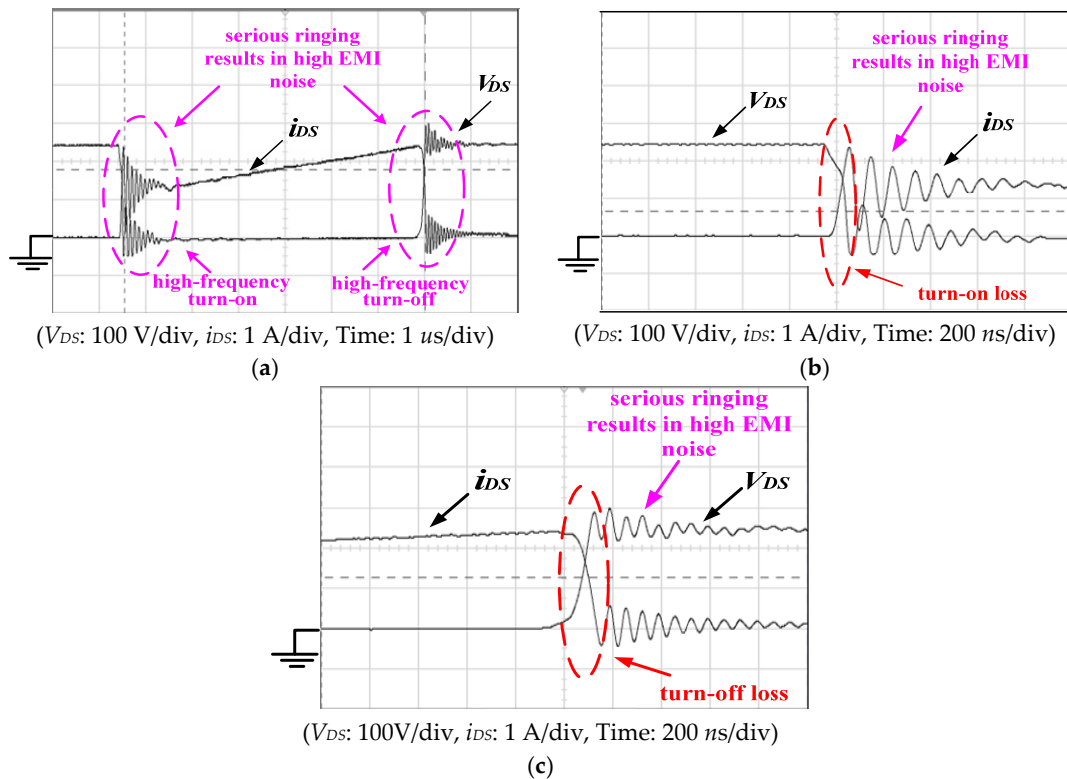


**Figure 2.** Experimental results of the power switch (Metal-oxide-semiconductor-field-effect transistor, MOSFET) with hard-switching conditions: (a) at turn-on and turn-off transitions; (b) extended waveforms of high turn-on loss and high electromagnetic interference (EMI); (c) extended waveforms of high turn-off loss and high EMI.

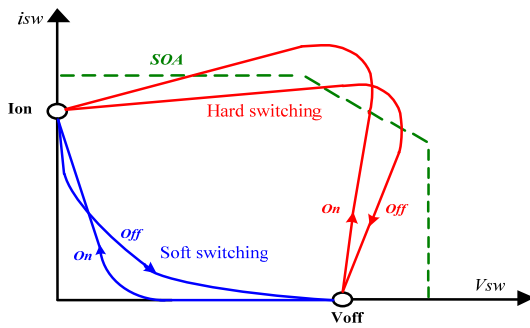


**Figure 3.** Switching loci of hard switching and soft switching for a power switch.

In general, the soft-switching techniques can be classified into zero-voltage-switching (ZVS) and zero-current-switching (ZCS) techniques [12–17]. The ZVS or ZCS techniques drive the voltage or current of the power switch to zero before any switching action, and avoids the concurrent high voltage and high current in the switching transition. The ZVS techniques include ZVS turn-on and ZVS turn-off transitions, as shown in Figure 4. As illustrated in Figure 4a, the ZVS turn-off technique is generally accomplished by slowing the voltage rising rate while the power switch is turning off. In order to reduce turn-off loss of the power switch, an extra capacitor is added to the power switch in parallel, as shown in Figure 5. However, the charge stored in the capacitor will be discharging through the power switch when the switch is turned on again, creating an extra conduction loss in the power switch. To release this loss, a zero-voltage turn-on technique is adopted. In general, the ZVS turn-on technique is without an added external capacitor on the power switch. Thus, the power switch has no extra conduction loss. Figure 4b illustrates the typical voltage and current of switches with the ZCS turn-on and turn-off operation. Power switches with ZCS have no current at the switch turn-on and turn-off transition to reduce the switching loss. To achieve ZCS turn-off conduction, the power switch must be incorporated as an external snubber circuit. The snubber circuit needs at least a capacitor, a diode, and an inductor, as shown in Figure 6. Thus, the complexity of the converter is increased. To resolve this disadvantage, the ZCS turn-on technique can be easily achieved by inserting an inductor in series with the power switch to limit the current rising rate at the switching transition. Comparing the ZVS/ZCS turn-on and ZVS/ZCS turn-off techniques, the ZVS/ZCS turn-on techniques have less components and are easily accomplished.

From the above description, power converters with ZVS/ZCS turn-on techniques are effective means for solving or alleviating switching losses and EMI problems [18–22]. In this paper, a soft-switching SEPIC with multi-output sources is proposed, as shown in Figure 7. The proposed soft-switching SEPIC has the following advantages: (1) The use of a simple flyback-type cell, which can achieve the ZVS turn-on condition of the main switch ( $M_1$ ) and the ZCS turn-on condition of the auxiliary switch ( $M_2$ ), resulting in low switching losses and EMI, and (2) To apply the voltage ratio of the transformers, the proposed SEPIC has the functions of multi-output sources with step-up/down voltage. In this paper, the power estimation of hard-switching SEPIC is described in Section 2. The operational principles of the proposed soft-switching SEPIC with multi-output sources are described in Section 3. Simulated and experimental results obtained from the proposed soft-switching SEPIC with multi-output sources are presented in Section 4. Finally, a conclusion is given in Section 5.

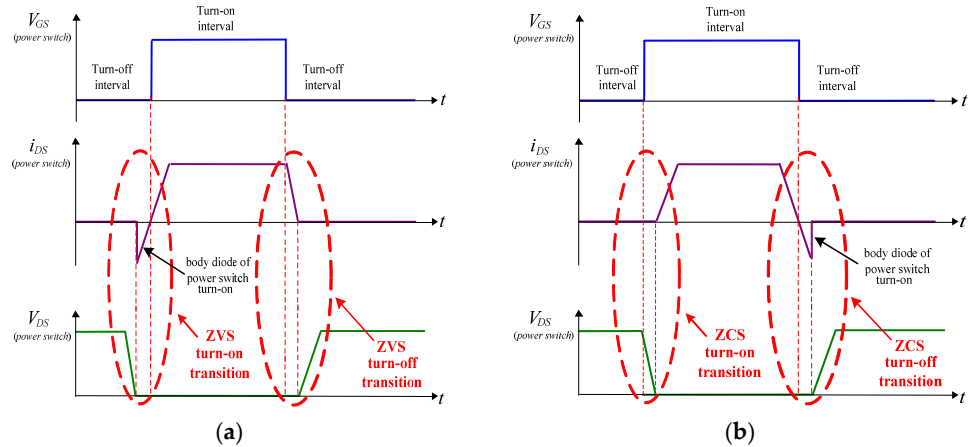


**Figure 4.** Illustration of ZVS (zero-voltage-switching) and ZCS (zero-current-switching) for a power switch: (a) ZVS turn-on and turn-off transitions; (b) ZCS turn-on and turn-off transitions.

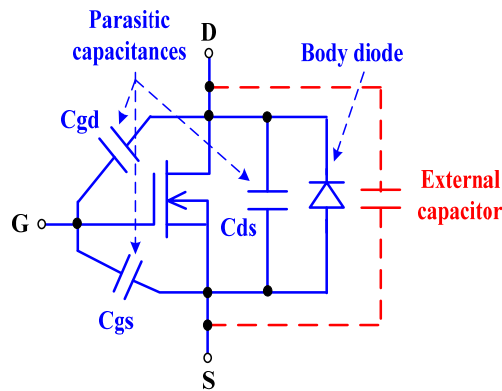


**Figure 5.** Illustration of the power switch in parallel with an extra capacitor.

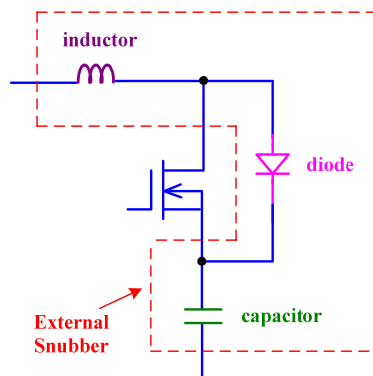


**Figure 6.** Illustration of the ZCS turn-off with an external snubber circuit.

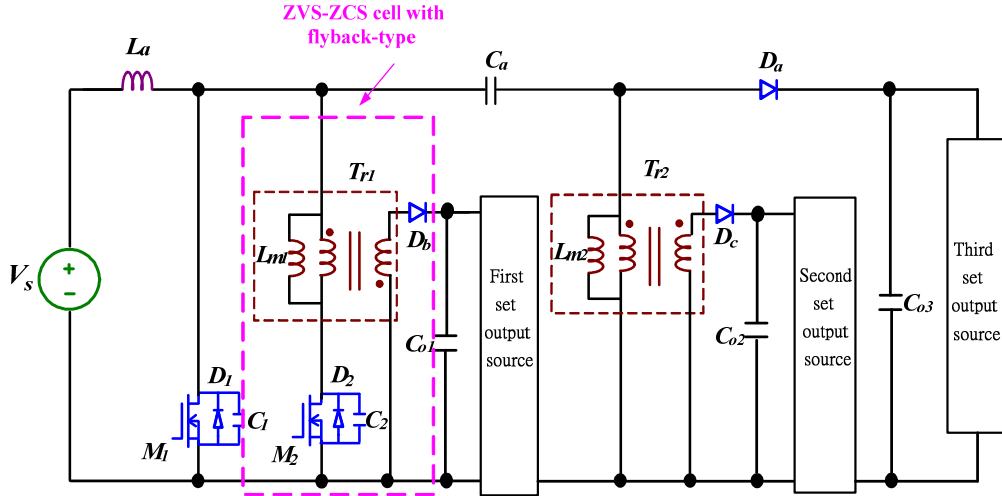


**Figure 7.** Topology of the soft-switching SEPIC with multi-output sources.

## 2. Power Estimation of Hard-Switching SEPIC

Figure 2 shows that the SEPIC with hard switching techniques results in serious EMI and high switching losses. The illustrated switching waveforms of the power switches are shown in Figure 8. The average switching power and conduction power losses over one switching cycle from the waveforms of Figure 8 can be evaluated as follows:

$$P_{ave} = \frac{1}{T} \left[ \int_0^T i_{sw} v_{sw} dt \right] = P_{ave,swit} + P_{ave,cond}, \quad (1)$$

where  $P_{ave,swit}$  is the average switching losses,  $P_{ave,cond}$  is the average conduction losses, and  $T$  is the switching cycle. The power losses of  $P_{ave,swit}$  and  $P_{ave,cond}$  can be expressed as follows:

$$P_{ave,swit} = \frac{1}{T} \left[ \int_0^{t_{on}} i_{sw} v_{sw} dt + \int_{DT-t_{off}}^{DT} i_{sw} v_{sw} dt \right], \quad (2)$$

$$\begin{aligned} P_{ave,cond} &= \frac{1}{T} \left[ \int_{t_{on}}^{DT-t_{off}} I_{on} V_{off} dt + \int_{DT}^T I_{off} V_{on} dt \right] \\ &= I_{on} V_{off} \left[ D - \frac{(t_{on}+t_{off})}{T} + I_{off} V_{on} (1-D) \right], \end{aligned} \quad (3)$$

where  $DT$  is the duty cycle and  $I_{off}$  is the leakage current of the power switch. If the on and off times are small compared to  $T$ , then Equation (3) can be expressed as follows:

$$P_{ave,cond} = I_{on} V_{off} D + I_{off} V_{on} (1-D). \quad (4)$$

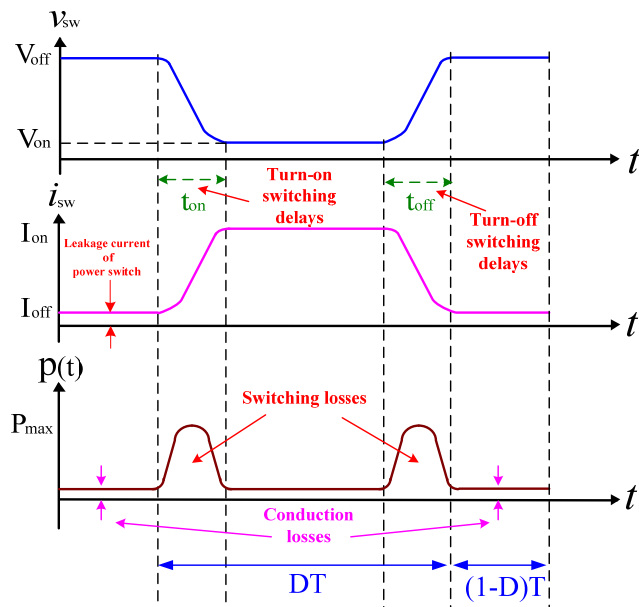


**Figure 8.** Illustration of the switch current, voltage, and power waveforms.

From Equation (2), it can be seen that the power losses of the power switch is operated at each cycle of the turn-on and turn-off transitions. Therefore, power converters with soft-switching techniques make them suitable for high-frequency operation. The benefits of power converters with ZVS and ZCS features can be summarized as follows:

- (1) Low switching losses and high conversion efficiency,
- (2) Low  $di/dt$  and  $dv/dt$ , and thus low voltage spikes and EMI emissions, and
- (3) High reliability and low cost.

### 3. Operational Principles

As shown in Figure 7, the proposed soft-switching SEPIC with multi-output sources consists of the main switch ( $M_1$ ), auxiliary switch ( $M_2$ ), transformers ( $T_{r1}$  and  $T_{r2}$ ), free-wheeling diodes ( $D_a$ ,  $D_b$ , and  $D_c$ ), and filter capacitors ( $C_a$ ,  $C_{o1}$ ,  $C_{o2}$ , and  $C_{o3}$ ). The soft-switching cell is composed of an auxiliary switch ( $M_2$ ) and a transformer ( $T_{r1}$ ) to achieve ZVS and ZCS features of the main and auxiliary switches ( $M_1$  and  $M_2$ ). Furthermore, to apply the voltage ratio of the transformers ( $T_{r1}$  and  $T_{r2}$ ), the proposed soft-switching SEPIC has multi-output sources with step-up/down voltage functions. Therefore, the utility of the proposed soft-switching SEPIC can be increased.

In Figure 7, the operational principles of the soft-switching SEPIC with multi-output sources over one switching cycle can be divided into seven major operating modes. Figure 9 shows the current and voltage waveforms of the key components and the driving signal switches ( $M_1$  and  $M_2$ ). Figure 10 shows the equivalent circuit modes of the soft-switching SEPIC with multi-output sources over a switching cycle. To simplify the description of the operational modes, the following assumptions are made.

- (1) Capacitances of  $C_a$ ,  $C_{o1}$ ,  $C_{o2}$ , and  $C_{o3}$  are large enough that the voltages across them are constant over a switching cycle.
- (2) All of the switching devices, MOSFETs, and diodes are ideal.

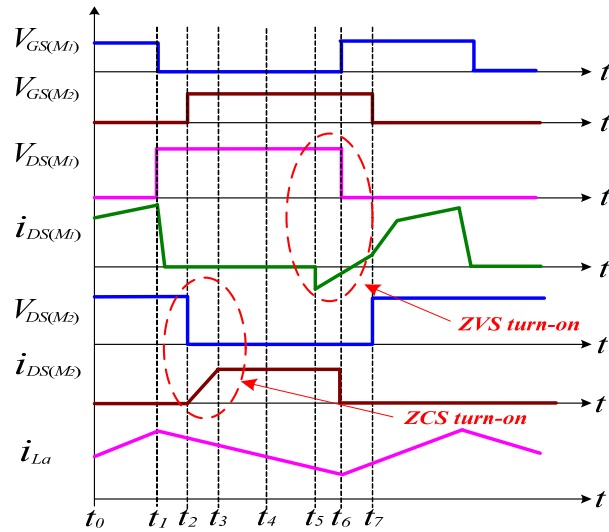


**Figure 9.** Current and voltage waveforms of the key components and the driving signal switches ( $M_1$  and  $M_2$ ) for the proposed soft-switching SEPIC.

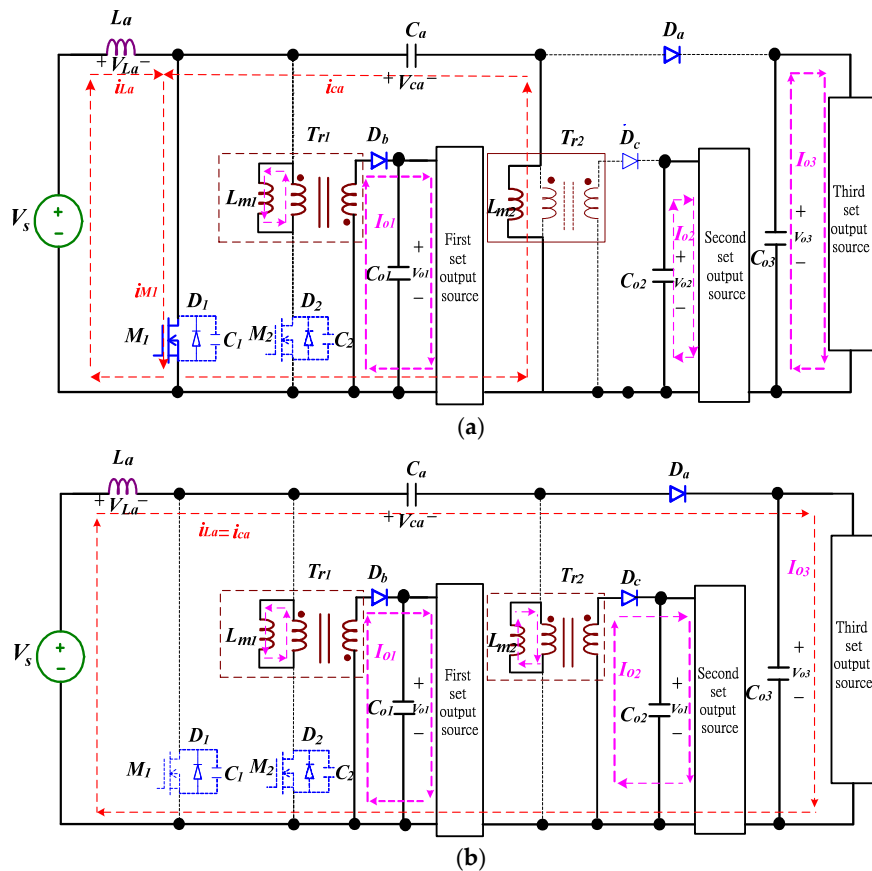


**Figure 10. Cont.**

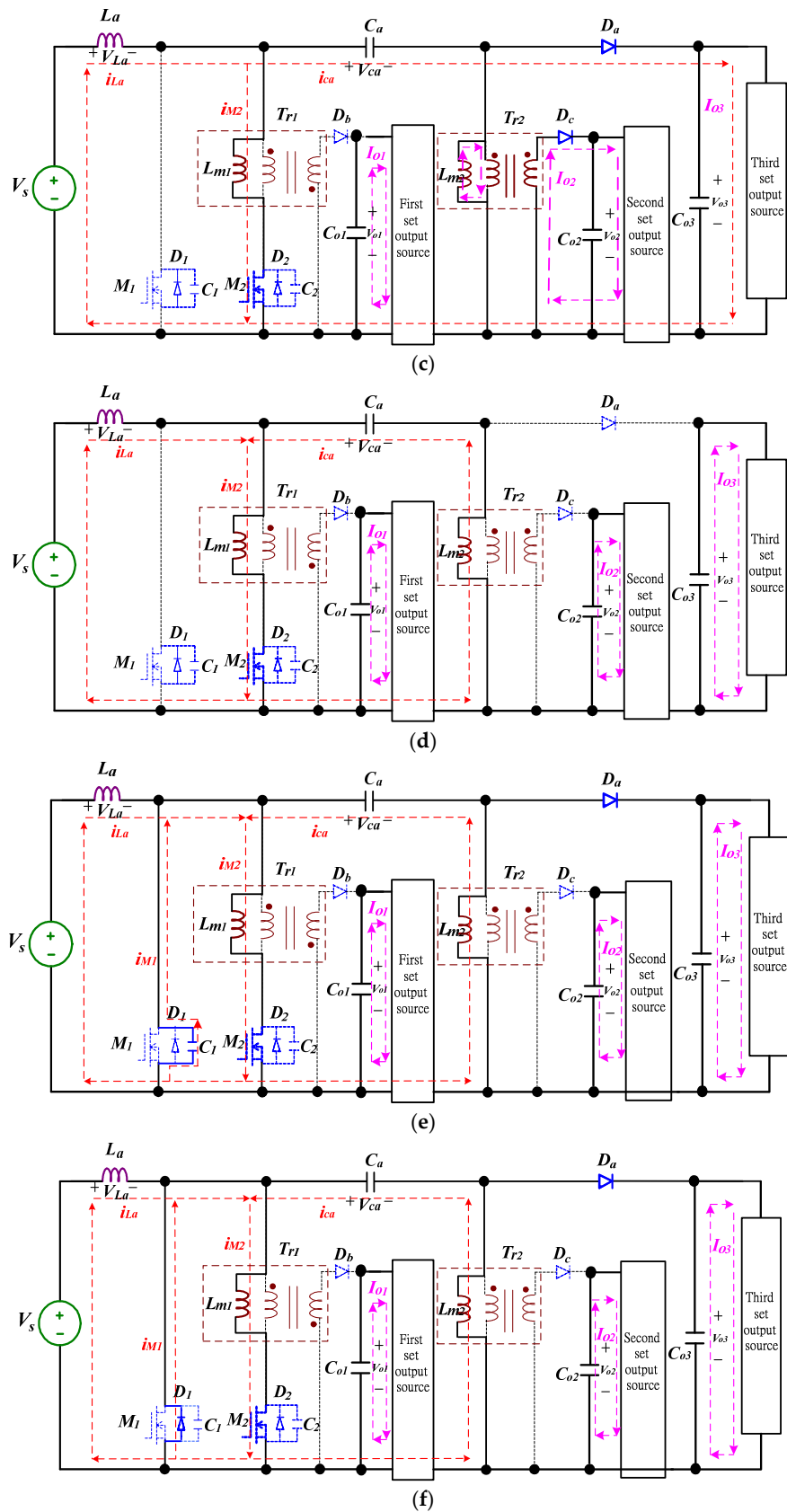
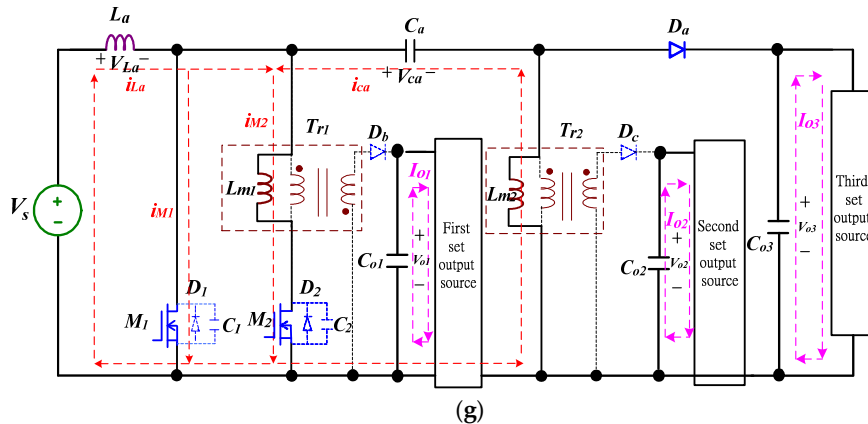


Figure 10. Cont.



**Figure 10.** Equivalent circuits of the soft-switching SEPIC with multi-output sources. (a) Mode 1; (b) Mode 2; (c) Mode 3; (d) Mode 4; (e) Mode 5; (f) Mode 6; (g) Mode 7.

#### Mode 1 (Figure 10a, $t_0 < t < t_1$ ):

At time  $t_0$ , the main switch ( $M_1$ ) is turned on and the auxiliary switch ( $M_2$ ) is turned off. The inductor current  $i_{L_a}$  flowing through the path of  $V_s-L_a-M_1$  linearly increases. The inductor current  $i_{L_a}$  can be expressed as follows:

$$i_{L_a}(t) = \frac{V_s}{L_s}(t - t_0). \quad (5)$$

While the capacitor ( $C_a$ ) is discharged, the discharging current  $i_{ca}$  is flowing through the path of  $C_a-M_1-T_{r2}$ . The current  $i_{ca}$  can be expressed as follows:

$$i_{ca}(t) = \frac{V_{Lm2}}{L_{m2}}(t - t_0). \quad (6)$$

At this time, the total current flowing through the main switch ( $M_1$ ) is  $i_{M1} = i_{L_a} + i_{ca}$ . During this mode, the freewheeling diodes ( $D_a$ ) and ( $D_c$ ) are turned off, and ( $D_b$ ) is turned on. The magnetic inductance ( $L_{m1}$ ) of the transformer ( $T_{r1}$ ) delivers power to the first-set source, and the capacitors ( $C_{o2}$  and  $C_{o3}$ ) individually deliver power to the second-set and third-set output sources. The equivalent circuit is shown in Figure 10a.

#### Mode 2 (Figure 10b, $t_1 < t < t_2$ ):

At time  $t_1$ , the main switch ( $M_1$ ) is turned off, and the auxiliary switch ( $M_2$ ) is kept off. While the freewheeling diode ( $D_a$ ) is turned on, the inductor current  $i_{L_a}$  begins discharging and flowing through the path of  $L_a-C_a-D_a-V_{o3}-V_s$  to deliver power to the third-set output source. The inductor current  $i_{L_a}$  can be expressed as follows:

$$i_{L_a}(t) = i_{ca}(t) = \frac{V_{ca} + V_{o3} - V_s}{L_a}(t - t_1). \quad (7)$$

During this interval, the freewheeling diodes ( $D_b$ ) and ( $D_c$ ) are turned on. The magnetic inductance ( $L_{m1}$ ) and ( $L_{m2}$ ) of transformers ( $T_{r1}$  and  $T_{r2}$ ) individually deliver power to the first-set and second-set sources. The equivalent circuit is shown in Figure 10b.

#### Mode 3 (Figure 10c, $t_2 < t < t_3$ ):

At time  $t_2$ , the auxiliary switch ( $M_2$ ) is turned on under the ZCS condition and the main switch ( $M_1$ ) is maintained off. The inductor current  $i_{L_a}$  is divided into two-branched currents  $i_{M2}$  and  $i_{ca}$ .

One is flowing through the path of  $L_a$ - $C_a$ - $D_a$ - $V_{o3}$ - $V_s$ , and the other is flowing through the path of  $L_a$ - $T_{r1}$ - $M_2$ - $V_s$ . The currents of  $i_{La}$ ,  $i_{M2}$ , and  $i_{ca}$  can be expressed as follows:

$$i_{La}(t) = i_{M2}(t) + i_{ca}(t), \quad (8)$$

$$i_{M2}(t) = \frac{(V_s + V_{La})}{L_{m1}}(t - t_2), \quad (9)$$

and

$$i_{ca}(t) = \frac{(V_s + V_{La} - V_{o3})}{L_a}(t - t_2). \quad (10)$$

During this interval, the freewheeling diode ( $D_b$ ) is turned off and ( $D_a$  and  $D_c$ ) are kept on. Capacitor ( $C_{o1}$ ) delivers power to the first-set source and the magnetic inductance ( $L_{m2}$ ) of transformer ( $T_{r2}$ ) delivers power to the second-set source. The equivalent circuit is shown in Figure 10c.

#### Mode 4 (Figure 10d, $t_3 < t < t_4$ ):

At time  $t_3$ , when current  $i_{La} = i_{M2}$ , the freewheeling diodes ( $D_a$  and  $D_c$ ) are turned off. Then, capacitor ( $C_a$ ) begins discharging through the path of  $C_a$ - $T_{r1}$ - $M_2$ - $T_{r2}$ . The currents of  $i_{La}$  and  $i_{ca}$  can be expressed as follows:

$$i_{La}(t) = \frac{(V_s + V_{La})}{L_{m1}}(t - t_3), \quad (11)$$

and

$$i_{ca}(t) = \frac{(V_s + V_{La} - V_{Lm2})}{L_{m1} + L_{m2}}(t - t_3). \quad (12)$$

At this time, the current  $i_{M2} = i_{La} + i_{ca}$ . During this interval, the capacitors ( $C_{o1}$ ,  $C_{o2}$ , and  $C_{o3}$ ) individually deliver power to the first-set, second-set, and third-set sources. The equivalent circuit is shown in Figure 10d.

#### Mode 5 (Figure 10e, $t_4 < t < t_5$ ):

At time  $t_4$ , when the current  $i_{La}$  is less than  $i_{M2}$ , the parasitic capacitance ( $C_1$ ) of the main switch ( $M_1$ ) is discharged. At this time, the current  $i_{M2} = i_{La} + i_{M1} + i_{ca}$ . The currents of  $i_{La}$  and  $i_{ca}$  can be expressed as follows:

$$i_{La}(t) = \frac{(V_s + V_{La} + V_{Lm1})}{L_{m1}}(t - t_4), \quad (13)$$

and

$$i_{ca}(t) = \frac{(V_{Lm1} + V_{Lm2})}{L_{m1} + L_{m2}}(t - t_4). \quad (14)$$

During this interval, the freewheeling diodes ( $D_a$ ,  $D_b$ , and  $D_c$ ) are kept off. The capacitors ( $C_{o1}$ ,  $C_{o2}$ , and  $C_{o3}$ ) individually deliver power to the first-set, second-set, and third-set sources. The equivalent circuit is shown in Figure 10e.

#### Mode 6 (Figure 10f, $t_5 < t < t_6$ ):

At time  $t_5$ , the voltage of the parasitic capacitor ( $C_1$ ) is dropped to zero, and the body diode of the main switch ( $M_1$ ) is conducting and creating a ZVS condition for the main switch ( $M_1$ ). At this time, the current  $i_{M2} = i_{La} + i_{M1} + i_{ca}$ . The currents of  $i_{La}$  and  $i_{ca}$  can be expressed as follows:

$$i_{La}(t) = \frac{V_s}{L_{m1}}(t - t_5), \quad (15)$$

and

$$i_{ca}(t) = \frac{(V_{Lm1} + V_{Lm2})}{L_{m1} + L_{m2}}(t - t_5). \quad (16)$$

During this interval, the freewheeling diodes ( $D_a$ ,  $D_b$  and  $D_c$ ) are kept off. The capacitors ( $C_{o1}$ ,  $C_{o2}$ , and  $C_{o3}$ ) individually deliver power to the first-set, second-set, and third-set sources. The equivalent circuit is shown in Figure 10f.

#### Mode 7 (Figure 10g, $t_6 < t < t_7$ ):

At time  $t_6$ , the main switch ( $M_1$ ) is turned on under the ZVS conduction. At this time, the current of the main switch ( $M_1$ ) is reversed, and the current of the auxiliary switch ( $M_2$ ) is  $i_{M2} = i_{La} + i_{ca} - i_{M1}$ . The currents of  $i_{La}$  and  $i_{ca}$  can be expressed as follows:

$$i_{La}(t) = \frac{V_s}{L_{m1}}(t - t_6), \quad (17)$$

and

$$i_{ca}(t) = \frac{(V_{Lm1} + V_{Lm2})}{L_{m1} + L_{m2}}(t - t_6). \quad (18)$$

During this interval, the freewheeling diodes ( $D_a$ ,  $D_b$ , and  $D_c$ ) are kept off. The capacitors ( $C_{o1}$ ,  $C_{o2}$ , and  $C_{o3}$ ) individually deliver power to the first-set, second-set, and third-set sources. The operational mode of the soft-switching SEPIC over one switching cycle is completed. The equivalent circuit is shown in Figure 10g.

## 4. Analysis of the Proposed Converter

In this section, the soft-switching cell and voltage gain of the proposed SEPIC with multi-output sources will be analyzed in detail.

### 4.1. Derivations of a ZVS-ZCS Cell with Flyback-Type

In the literature, a number of power converters with soft-switching cells have been proposed [23–31]. All of them employ an auxiliary switch and passive components to form a soft-switching cell, which is used only to create a condition for achieving ZVS and ZCS at the power switches' turn-on transition. Figure 11 shows an equivalent power converter with a soft-switching cell. The topology differs from a conventional power converter by an additional auxiliary switch ( $M_2$ ) and a resonant inductor ( $L_1$ ) which includes the parasitic capacitor ( $C_1$ ) of the main switch ( $M_1$ ) and a freewheeling diode ( $D_a$ ). This resonant branch  $L_1-M_2-C_1$  is active only during a short switching transition time to create a ZVS condition for the main switch ( $M_1$ ) and a ZCS condition for the auxiliary switch ( $M_2$ ). By incorporating this type of resonant network, the soft-switching concept can be extended to generate different ZVS-ZCS types of power converters.

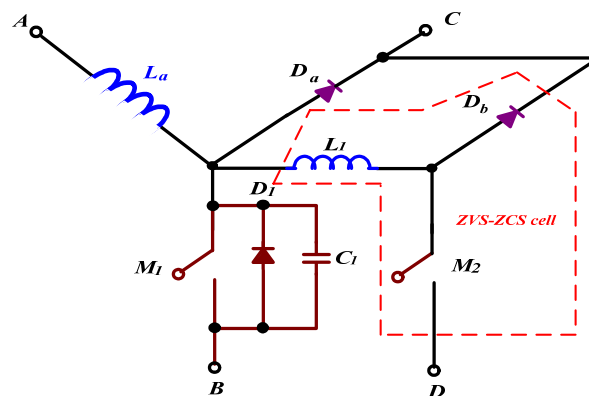


**Figure 11.** Topology of an equivalent power converter with a soft-switching cell.

Figure 12 shows a conventional SEPIC with a ZVS-ZCS inductor-type cell. The ZVS-ZCS inductor-type cell is composed of a resonant inductor ( $L_1$ ), an auxiliary switch ( $M_2$ ) and a diode ( $D_b$ ), which operates at a fixed frequency and is controlled by a pulse-width-modulated (PWM) scheme. In Figure 12, to obtain multi-output sources and increase utility, the resonant inductor ( $L_1$ ) of the ZVS-ZCS cell and the inductor ( $L_b$ ) can be replaced by transformers. Therefore, the ZVS-ZCS cell and the inductor ( $L_b$ ) of Figure 13 can be modified to use two sets of flyback cell. Finally, a soft-switching SEPIC with multi-output sources is obtained, as shown in Figure 7.

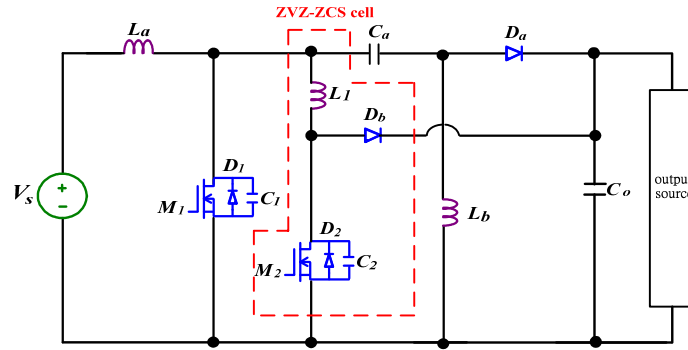


**Figure 12.** Topology of a conventional SEPIC with an inductor-type ZVS-ZCS cell.

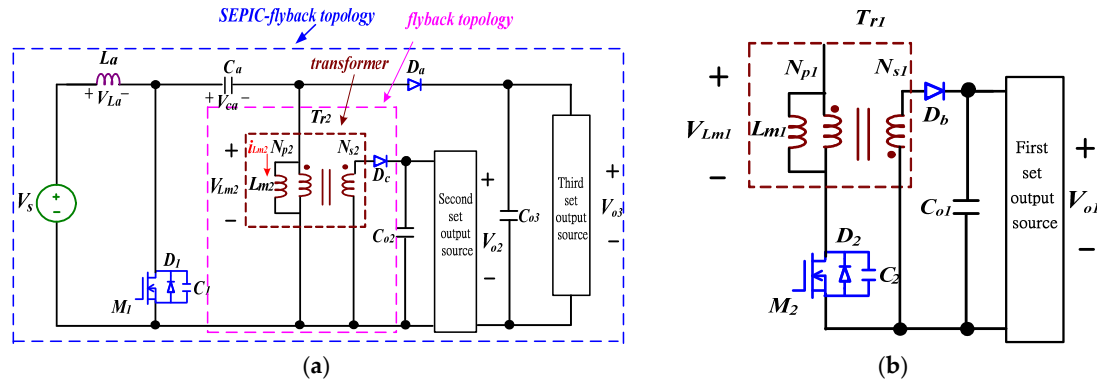


**Figure 13.** Illustration of two topologies for the proposed converter: (a) SEPIC-flyback topology; (b) flyback topology.

#### 4.2. Analysis of the Voltage Gain

The proposed soft-switching SEPIC has three sets of output sources, as shown in Figure 7. In order to obtain a facile analysis, the proposed soft-switching SEPIC with multi-output sources can be divided into two topologies. One is the SEPIC-flyback topology, and the other is the flyback topology, as shown in Figure 13.

In Figure 13a, it can be seen that the SEPIC-flyback topology is a combination of a SEPIC and a flyback converter. In order to obtain a facile analysis, the currents of inductor ( $L_a$ ) of the SEPIC are assumed to be continuous. When the switch ( $M_1$ ) is turned on and the diode ( $D_a$ ) is turned off, the voltage across the inductor ( $L_a$ ) is expressed as:

$$V_{L_a(\text{switch turn-on})} = V_s. \quad (19)$$

When the switch ( $M_1$ ) is turned off and the diode ( $D_a$ ) is turned on, the voltage across the inductor ( $L_a$ ) is expressed as:

$$V_{L_a(\text{switch turn-off})} = V_{c1} + V_{o3} - V_s. \quad (20)$$

In steady-state operation, the voltage ( $V_{ca}$ ) across capacitor ( $C_a$ ) remains constant and can be expressed as:

$$V_{c1} = V_s. \quad (21)$$

Therefore, Equation (5) can be expressed as:

$$V_{La,(switch\ turn-off)} = V_{o3}. \quad (22)$$

According to the volt-second balance principle of the inductor ( $L_a$ ), the average voltage across an inductor is zero for a periodic operation. Equations (4) and (7) are combined to obtain the following:

$$V_{La,(switch\ turn-on)}(DT) = V_{La,(switch\ turn-off)}(1 - D)T, \quad (23)$$

or

$$V_s(DT) = V_{o3}(1 - D)T, \quad (24)$$

where  $D$  is the duty ratio of the switch ( $M_1$ ), and the result of the voltage gain for the output source of the third set can be determined as:

$$\frac{V_{o3}}{V_s} = \frac{D}{1 - D}. \quad (25)$$

For the output source of the secondary, the voltage gain can be determined by the volt-second balance principle. When the switch ( $M_1$ ) is turned on and the diode ( $D_a$ ) is turned off, energy is stored in the magnetizing inductance ( $L_{m2}$ ) of transformer ( $T_{r2}$ ). The voltage of the magnetizing inductance ( $L_{m2}$ ) is expressed as:

$$V_{Lm2,(switch\ turn-on)} = V_{c1} = V_s. \quad (26)$$

When the switch ( $M_1$ ) is turned off and the diode ( $D_a$ ) is turned on, the current of the magnetizing inductance ( $L_{m2}$ ) cannot change instantaneously. Therefore, the conduction path must be through the primary turns ( $N_{p2}$ ) of the transformer ( $T_{r2}$ ). The current  $i_{Lm2}$  enters the dotted terminal of the primary and must exit from the dotted terminal of the secondary. The secondary voltage  $V_{s2}$  of the transformer ( $T_{r2}$ ) becomes  $V_{o2}$ . The secondary voltage  $V_{s2}$  of the transformer ( $T_{r2}$ ) is sent back to the primary and establishes the voltage across the magnetizing inductance ( $L_{m2}$ ), which is expressed as:

$$V_{Lm2,(switch\ turn-off)} = V_{o2}\left(\frac{N_{p2}}{N_{s2}}\right), \quad (27)$$

where  $N_{p2}$  is the primary turns and  $N_{s2}$  is the secondary turns of transformer ( $T_{r2}$ ). According to the volt-second balance principle of the magnetizing inductor ( $L_{m2}$ ), the average voltage across the primary turns ( $N_{p2}$ ) and secondary turns ( $N_{s2}$ ) is zero for a periodic operation. Equations (11) and (12) are combined to obtain the following:

$$V_{Lm2,(switch\ turn-on)}(DT) = V_{Lm2,(switch\ turn-off)}(1 - D)T, \quad (28)$$

or

$$V_s DT = V_{o2}\left(\frac{N_{p2}}{N_{s2}}\right)(1 - D)T. \quad (29)$$

The result of the voltage gain for the output source of the secondary set can be determined as:

$$\frac{V_{o2}}{V_{Lm2}} = \left(\frac{N_{s2}}{N_{p2}}\right)\left(\frac{D}{1 - D}\right). \quad (30)$$

Similarly, Figure 13b is also a flyback topology. According to Equations (12)–(15), the result of the voltage gain for the output source of the first set can be determined as:

$$\frac{V_{o1}}{V_{Lm1}} = \left( \frac{N_{s1}}{N_{p1}} \right) \left( \frac{D}{1-D} \right), \quad (31)$$

where  $N_{p1}$  is the primary turns and  $N_{s1}$  is the secondary turns of transformer ( $T_{r1}$ ).

#### 4.3. Region of ZVS and ZCS

To reduce switching losses and increase the conversion efficiency, the proposed SEPIC is incorporated with a soft-switching cell to implement ZVS and ZCS features. In Figure 7, the voltage across the main switch ( $M_1$ ) is larger than that across the auxiliary switch ( $M_2$ ). Thus, the magnetizing inductance ( $L_{m1}$ ) of the transformer ( $T_{r1}$ ) has enough energy to achieve the ZVS and ZCS features for the main switch ( $M_1$ ) and auxiliary switch ( $M_2$ ). To achieve the ZVS and ZCS features, the magnetizing inductance ( $L_{m1}$ ) of the transformer ( $T_{r1}$ ) needs to meet the following inequality:

$$L_{m1} \geq \frac{C_1(V_s + V_{La})^2}{(I_{o1}/n)^2}, \quad (32)$$

where  $n = N_{s1}/N_{p1}$  is the turns ratio of the transformer ( $T_{r1}$ ),  $I_{o1}$  is the average output current of the first-set source, and  $C_1$  is the parasitic capacitance of the main switch ( $M_1$ ). The ZVS and ZCS features for the main switch ( $M_1$ ) and auxiliary switch ( $M_2$ ) depend on  $C_1$ ,  $L_{m1}$ ,  $V_s$ , and  $I_{o1}$ . Therefore, we can plot the curves, showing the relationships between the magnetizing inductance ( $L_{m1}$ ) and the output current  $I_{o1}$  for different values of input voltage  $V_s$ , as illustrated in Figure 14. For achieving the ZVS and ZCS features, the magnetizing inductance ( $L_{m1}$ ) should be selected from the area above the grid surface, as shown in Figure 14.

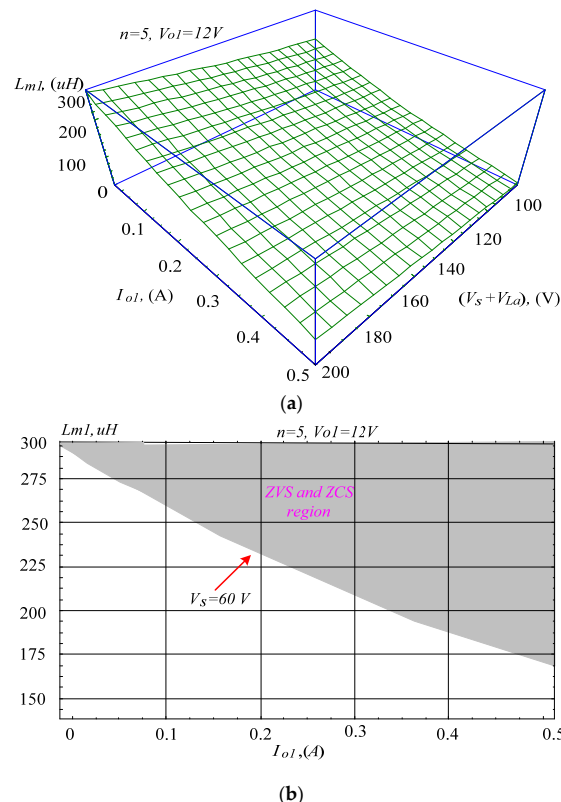


**Figure 14.** (a) 3-D plots of the minimum magnetizing inductance ( $L_{m1}$ ) of the transformer ( $T_{r1}$ ) as a function of the output current ( $I_{o1}$ ) under different input voltages for achieving ZVS and ZCS features; (b) a partial plot showing the ZVS and ZCS region versus the output current ( $I_{o1}$ ) at  $V_s = 60$  V.

## 5. Simulated and Experimental Results

To verify the feasibility of the design, a 150 W prototype of the proposed soft-switching SEPIC with multi-output sources is implemented. Its specifications are listed as follows:

- input voltage:  $V_s = 60 V_{dc}$ ,
- first-set output voltage:  $V_{o1} = 12 V_{dc}$ ,
- second-set output voltage:  $V_{o2} = 24 V_{dc}$ ,
- third-set output voltage:  $V_{o3} = 100 V_{dc}$ ,
- total output power: 150 W, and
- switching frequency:  $f = 55$  kHz.

Figure 15 shows the simulated and experimental voltage and current waveforms of the main switch ( $M_1$ ) at the turn-on transition for the proposed soft-switching SEPIC. From Figure 15, it can be seen that the main switch ( $M_1$ ) has a ZVS feature and low EMI noise. Figure 16 shows the simulated and experimental voltage and current waveforms of the auxiliary switch ( $M_2$ ) at the turn-on transition for the proposed soft-switching SEPIC. From Figure 16, it can be seen that the auxiliary switch ( $M_2$ ) also has a ZCS feature and low EMI noise. The experimental efficiency of the proposed multi-output sources SEPIC with soft-switching and hard-switching techniques are obtained in Figure 17. From which it can be seen that the maximum efficiency with soft-switching techniques can be as high as 90%. Compared with the hard-switching techniques, the proposed multi-output sources SEPIC with soft-switching techniques has low switching losses, low EMI, and high conversion efficiency.

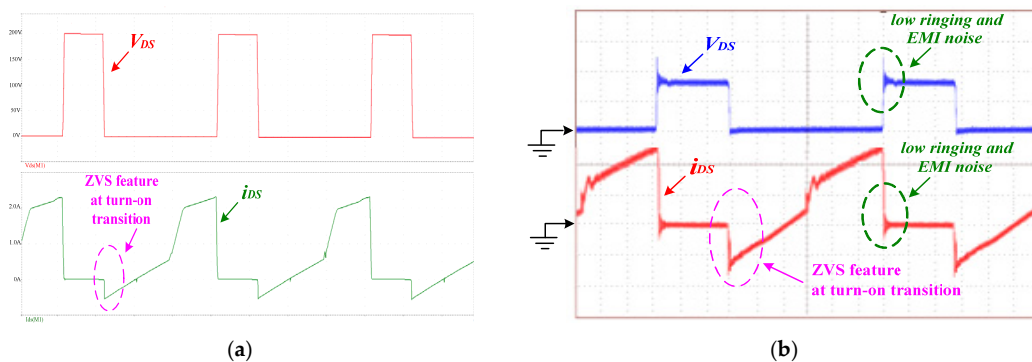


**Figure 15.** Voltage and current waveforms of the main switch ( $M_1$ ): (a) simulated results ( $V_{DS}$ : 50 V/div;  $i_{DS}$ : 1 A/div; Time: 5  $\mu$ s/div); (b) experimental results ( $V_{DS}$ : 100 V/div;  $i_{DS}$ : 1 A/div; Time: 2  $\mu$ s/div).

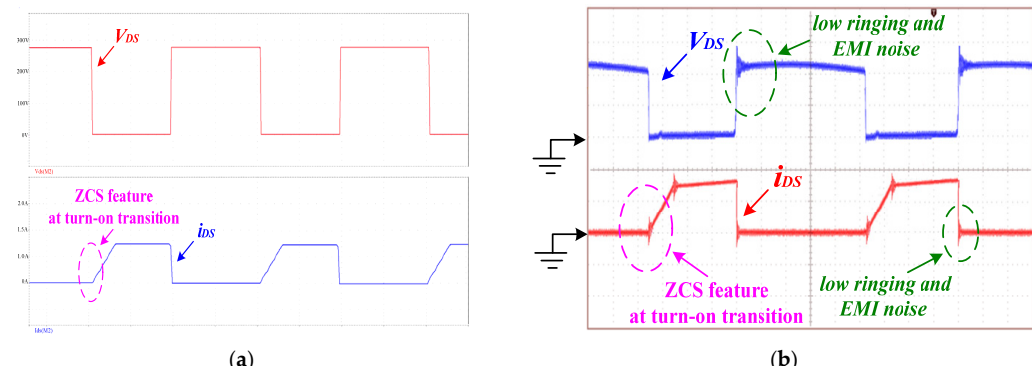


**Figure 16.** Voltage and current waveforms of the auxiliary switch ( $M_2$ ): (a) simulated results ( $V_{DS}$ : 100 V/div;  $i_{DS}$ : 0.5 A/div; Time: 5  $\mu$ s/div); (b) experimental results ( $V_{DS}$ : 100 V/div;  $i_{DS}$ : 0.5 A/div; Time: 2  $\mu$ s/div).

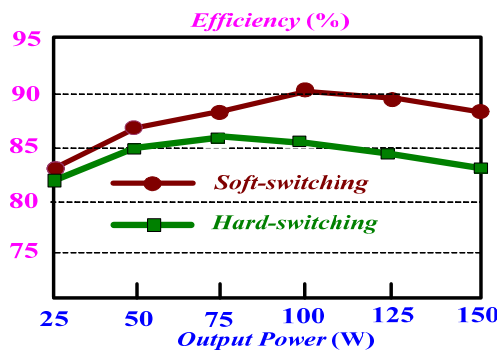


**Figure 17.** Efficiency of the proposed multi-output sources SEPIC with soft-switching and hard-switching techniques under full load condition.

## 6. Conclusions

In this paper, the proposed soft-switching SEPIC with multi-output sources has been built and implemented. It uses a soft-switching cell with flyback-type to implement the features of ZVS and ZCS under turn-on transitions for the main switch ( $M_1$ ) and the auxiliary switch ( $M_2$ ). Therefore, the switching losses and EMI of the main and auxiliary switches can be reduced, and the efficiency can be increased. In addition, to apply the voltage ratios of the transformers ( $T_{r1}$  and  $T_{r2}$ ), the proposed soft-switching SEPIC has multi-output sources with step-up/down voltage functions. Therefore, the utility of the proposed soft-switching SEPIC can be increased. The simulated and experimental results have verified that the proposed soft-switching SEPIC with multi-output sources is relatively suitable for renewable energy systems.

**Acknowledgments:** This work was supported by the Ministry of Science and Technology, Taiwan, under Grant No. MOST 105-2221-E-167-023.

**Author Contributions:** All of the authors contributed to the publication of this paper. Cheng-Tao Tsai wrote the paper; Jye-Chau Su edited the manuscript.

**Conflicts of Interest:** The authors declare no conflict of interest.

## References

- Shen, C.L.; Tsai, C.T. Double-linear approximation algorithm to achieve maximum-power-point tracking for photovoltaic arrays. *Energies* **2012**, *5*, 1982–1997. [[CrossRef](#)]
- Vasilij, J.; Sarajcev, P.; Jakus, D. Estimating Future Balancing Power Requirements in Wind-PV Power System. *Renew. Energy* **2016**, *99*, 369–378. [[CrossRef](#)]
- Adhikari, J.; Prasanna, I.V.; Panda, S.K. Power Conversion System for High Altitude Wind Power Generation with Medium Voltage AC Transmission. *Renew. Energy* **2016**, *92*, 562–578. [[CrossRef](#)]
- Tsai, C.T.; Chen, W.M. Buck Converter with Soft-Switching Cells for PV Panel Applications. *Energies* **2016**, *9*, 148. [[CrossRef](#)]
- Ridley, R. *Analyzing the SEPIC Converter*; Power Systems Design Europe: Roswell, NM, USA, 2006; pp. 14–18.
- Axelrod, B.; Berkovich, Y. New Coupled-Inductor SEPIC Converter with Very High Conversion Ratio and Reduced Voltage Stress on the Switches. In Proceedings of the 2011 IEEE 33rd International Telecommunications Energy Conference (INTELEC), Amsterdam, The Netherlands, 9–13 October 2011; pp. 1–7.
- Gu, W.; Zhang, D. *Designing a SEPIC Converter*; Excellent Design Guidelines, National Semiconductor in Application Note: Los Angeles, CA, USA, 2008; pp. 1–6.
- Ali, M.; Orabi, M.; Ahmed, M.E.; El-Aroudi, A. Design Consideration of Modified SEPIC Converter for LED Lamp Driver. In Proceedings of the 2010 2nd IEEE International Symposium on Power Electronics for Distributed Generation Systems (PEDG), Heifei, China, 16–18 June 2010; pp. 394–399.
- Do, H.L. Soft-Switching SEPIC Converter with Ripple-Free Input Current. *IEEE Trans. Power Electron.* **2012**, *27*, 2879–2887. [[CrossRef](#)]

10. Chen, S.M.; Liang, T.J.; Yang, L.S.; Chen, J.F. A Cascaded High Step-up DC–DC Converter with Single Switch for Micro source Applications. *IEEE Trans. Power Electron.* **2011**, *26*, 1146–1153. [[CrossRef](#)]
11. Hu, J.; Sagneri, A.D.; Rivas, J.M.; Davis, S.M.; Perreault, D.J. High Frequency Resonant Sepic Converter with Wide Input and Output Voltage Ranges. In Proceedings of the 2008 IEEE Power Electronics Specialists Conference, Rhodes, Greece, 15–19 June 2008; pp. 1397–1406.
12. Wang, C.M. New Family of Zero-Current-Switching PWM Converters Using a New Zero-Current-Switching PWM Auxiliary Circuit. *IEEE Trans. Ind. Electron.* **2006**, *53*, 768–777. [[CrossRef](#)]
13. Wu, X.; Zhang, J.; Ye, X.; Qian, Z. Analysis and Derivations for a Family ZVS Converter Based on a New Active Clamp ZVS Cell. *IEEE Trans. Ind. Electron.* **2008**, *55*, 773–781. [[CrossRef](#)]
14. Kavitha Unnikrishnan, C.; Reshma Raj, C. High Frequency Quasi Resonant SEPIC Converter for Wide Range of Operation. In Proceedings of the 2014 International Conference on Circuit, Power and Computing Technologies (ICCPCT), Tamil Nadu, India, 20–21 March 2014; pp. 984–989.
15. Ongaro, F.; Saggini, S. ZVS Isolated Active Clamp Sepic Converter for High Power LED Applications. In Proceedings of the 2012 Twenty-Seventh Annual IEEE Applied Power Electronics Conference and Exposition (APEC), Orlando, FL, USA, 5–9 February 2012; pp. 957–962.
16. Lin, B.R.; Shih, K.L.; Chen, J.J.; Chiang, H.K. Implementation of a Zero Voltage Switching Sepic-Cuk Converter. In Proceedings of the 2008 3rd IEEE Conference on Industrial Electronics and Applications, Singapore, 3–5 June 2008; pp. 394–399.
17. Silva Costa, P.J.; Illa Font, C.H.; Lazzarin, T.B. Improvement of Stability in Current-Programmed SEPIC DC/DC Converters. In Proceedings of the 2015 IEEE 13th Brazilian Power Electronics Conference and 1st Southern Power Electronics Conference (COBEP/SPEC), Fortaleza, CE, Brazil, 29 November–2 December 2015; pp. 1–6.
18. Maged, N.F. Design of a Digital PWM Controller for a Soft Switching SEPIC Converter. *J. Power Electron.* **2004**, *4*, 152–160.
19. Corradini, L. Zero voltage switching technique for bidirectional DC/DC converters. *IEEE Trans. Power Electron.* **2014**, *29*, 1585–1594. [[CrossRef](#)]
20. Elasser, A.; Torry, D.A. Soft Switching Active Snubbers for DC/DC Converters. *IEEE Trans. Power Electron.* **1996**, *11*, 710–722. [[CrossRef](#)]
21. Smith, K.M., Jr.; Smedley, K.M. Properties and Synthesis of Lossless, Passive Soft Switching Converters. In Proceedings of the 1st International Congress in Israel on Energy, Power & Motion Contrtol, Tel-Aviv, Israel, 5–6 May 1997; pp. 112–119.
22. Xu, D.H.; Chen, M.; Lou, J.; Luo, M. Transformer secondary leakage inductance based ZVS dual bridge DC/DC converter. *IEEE Trans. Power Electron.* **2004**, *19*, 1408–1416. [[CrossRef](#)]
23. Tseng, C.-J.; Chen, C.-L. Passive Lossless Snubbers for DC/DC Converters. In Proceedings of the 1998 Thirteenth Annual Conference on Applied Power Electronics Conference and Exposition, Anaheim, CA, USA, 15–19 February 1998; pp. 1049–1054.
24. Watson, R.; Hua, G.; Lee, F.C. Characterization of an Active Clamp Flyback Topology for Power Factor Correction Applications. *IEEE Trans. Power Electron.* **1996**, *11*, 191–198. [[CrossRef](#)]
25. Duarte, C.M.C.; Barbi, I. A Family of ZVS-PWM Active-Clamping Dc-to-Dc Converters: Synthesis, Analysis, Design, and Experimentation. *IEEE Trans. Circuits Syst. I Fundam. Theory Appl.* **1997**, *44*, 698–704. [[CrossRef](#)]
26. Jitaru, I.D. Constant Frequency, Forward Converter with Resonant Transition. In Proceedings of the High Frequency Power Conversion Conference, Toronto, ON, Canada, 9–14 June 1991; pp. 282–292.
27. Liu, K.H.; Lee, F.C. Zero-Voltage Switching Technique in DC/DC Converter. *IEEE Trans. Power Electron.* **1990**, *5*, 293–304. [[CrossRef](#)]
28. Wang, H.; Chung, H.S.; Ioinovici, A. A New Concept of High-Voltage DC–DC Conversion Using Asymmetric Voltage Distribution on the Switch Pairs and Hybrid ZVS–ZCS Scheme. *IEEE Trans. Power Electron.* **2012**, *27*, 2242–2259. [[CrossRef](#)]
29. Wang, C.M. A Novel ZCS-PWM Flyback Converter with a Simple ZCS-PWM Commutation Cell. *IEEE Trans. Ind. Electron.* **2008**, *55*, 749–757. [[CrossRef](#)]

30. Chiang, C.; Chen, C. Zero-Voltage-Switching Control for a PWM Buck Converter under DCM/CCM Boundary. *IEEE Trans. Power Electron.* **2009**, *24*, 2120–2126. [[CrossRef](#)]
31. Lee, Y.S.; Chen, G.T. ZCS bi-directional DC-to-DC converter application in battery equalization for electric vehicles. In Proceedings of the IEEE Power Electronics Specialists Conference, Aachen, Germany, 20–26 June 2004; Volume 4, pp. 2766–2772.



© 2017 by the authors. Licensee MDPI, Basel, Switzerland. This article is an open access article distributed under the terms and conditions of the Creative Commons Attribution (CC BY) license (<http://creativecommons.org/licenses/by/4.0/>).